Mem. S.A.It. Suppl. Vol. 18, 133

Memorie della
Supplementi

Radial dependence in the pattern speed of M51 measured with the radial Tremaine-Weinberg method

S. E. Meidt[1], R. J. Rand[1], M. R. Merrifield[2], R. Shetty[3], and S. Vogel[4]

[1] Department of Physics and Astronomy, University of New Mexico, Albuquerque, NM, USA, e-mail: shmeidt@unm.edu
[2] School of Physics and Astronomy, University of Nottingham, Nottingham, UK
[3] Center for Astrophysics, Harvard University, Cambridge, MA, USA
[4] Department of Astronomy, University of Maryland, College Park, MD, USA

Abstract. We investigate evidence for radial variation in the spiral pattern speed of the grand-design spiral galaxy M51 using the radial Tremaine-Weinberg (TWR) method. We implement the method on CO observations tracing the ISM-dominant molecular component. Results from the method's numerical implementation–combined with regularization, which smooths intrinsically noisy solutions–indicate two distinct pattern speeds inside 4 kpc at our derived major axis PA = 170°, both ending at corotation and both significantly higher than the conventionally adopted global value. Inspection of the rotation curve suggests that the pattern speed interior to 2 kpc lacks an ILR, consistent with the leading structure seen in HST near-IR observations. We also find tentative evidence for a lower pattern speed between 4 and 5.3 kpc measured by extending the regularized zone. As with the original TW method, uncertainty in major axis position angle (PA) is the largest source of error in the calculation; in this study, where $\delta_{\rm PA} = \pm 5°$, a $\sim$ 20% error is introduced to the parameters of the speeds at PA = 170°.

Key words. galaxies: kinematics and dynamics – galaxies: spiral – galaxies: structure – methods: numerical

1. Introduction

The large angular size and clear spiral structure of the nearly face-on spiral M51 make it ideal for studies of the nature and origin of grand design spiral structure. Two scenarios dominate the discussion in the literature, each based on opposing theories: strong spiral structure as a quasi-stationary density wave (e.g., Lin & Shu 1964; see Elmegreen et al. 1989; Vogel et al. 1993; Rand 1993), or as a transient feature due to interaction with nearby companion NGC 5195 (e.g. Tully 1974; see Toomre & Toomre 1972; Howard & Byrd 1990; Salo & Laurikainen 2000a).

Knowledge of the pattern speed of the structure can, in principle, both distinguish between and reconcile the short- and long-lived wave scenarios, and so many studies have focused on measuring and characterizing this parameter (see Tully 1974; Elmegreen et al. 1989; Salo & Laurikainen

Send offprint requests to: S. Meidt

2000a; Garcìa-Burillo et al. 1993, for example). The pattern speed of the outer spiral has long been proposed near 10–20 $\mathrm{km\,s^{-1}\,kpc^{-1}}$ (i.e., Tully 1974). In the inner disk, application of the traditional, model-independent method of Tremaine & Weinberg (1984; hereafter TW) using CO observations yields a pattern speed $\Omega_\mathrm{p} = 38\ \mathrm{km\,s^{-1}\,kpc^{-1}}$ (Zimmer et al. 2004), in general agreement with the determinations based on resonance locations of Elmegreen et al. (1989) and Tully (1974) (but higher than the pattern speed Ω_p=27 $\mathrm{km\,s^{-1}\,kpc^{-1}}$ found by Garcìa-Burillo et al. 1993). Although the TW analysis shows evidence for significant departures from the expected relation for a constant pattern speed in both the inner- and outer-most regions of the disk, the method cannot quantitatively account for any suspected radial variation of the pattern speed.

The radial TW (hereafter TWR) method (Merrifield et al. 2006; Meidt et al. 2008a) proves to be an invaluable resource in this regard: with it we can characterize the angular speeds of distinct patterns and their possible radial variation. For the first time, we are able to observationally address issues related to the complex nature and persistence of spiral patterns and the connection, if any, between multiple pattern speeds in a single disk.

2. TWR method with regularization

The TWR method allows for the measurement of radially-dependent pattern speeds using observationally accessible quantities. The calculation proceeds under assumptions parallel to those of the original method (see Meidt et al. 2008b, for a review), but where there the disk is assumed to contain a single, well-defined rigidly rotating pattern, here Ω_p=$\Omega_\mathrm{p}(r)$ – and the surface density of the tracer $\Sigma(x, y, t) = \Sigma(r, \phi - \Omega_\mathrm{p}(r)t)$. Integration of the continuity equation obeyed by the tracer in this case yields a Volterra integral equation of the first kind for $\Omega_\mathrm{p}(r)$, which can be discretized for numerical solution for different values of r=r_j and y=y_i, taking the form of the matrix expression

$$K_{ij}\Omega_j = b_i. \quad (1)$$

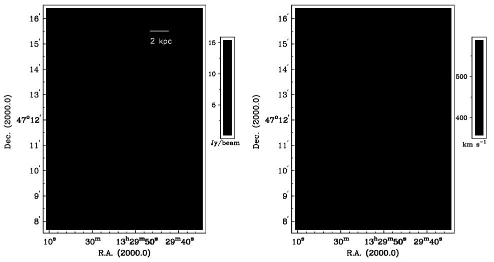

Fig. 1. Zeroth (right) and first (left) moment maps of the M51 CO cube (originally presented in Shetty et al. 2007). The $y > 0$ quadrature generally covers the eastern half of the image (depending on the value of the PA adopted), while the $y < 0$ quadrature covers the western.

Here $\mathbf{K}$ is an upper triangular $N \times N$ square matrix and $b_i = \langle v \rangle_i \int_{-\infty}^{\infty} \Sigma\, dx$, both related to the familiar TW Σ-weighted position $\langle x \rangle$ and velocity $\langle v \rangle$ calculated along slices at positions y, respectively.

Eq. 1 can be solved numerically for a total of two independent measures of $\Omega_\mathrm{p}(r)$, one from either side of the galaxy ($y > 0$ and $y < 0$). Here we solve for Ω_j using the regularization technique described in Meidt et al. (2008a), which reduces the intrinsic propagation of noise in solutions while maintaining the precision required to accurately identify true radial variation. The calculation in this case incorporates a priori models for the radial dependence of the pattern speed.

As in Meidt et al. (2008a), the best fit global solution constructed from the average of like-model solutions from the two sides is established with the standard χ^2 per degree of freedom statistic. For this statistic we adopt errors $\sigma_i^{\langle v \rangle}$ that reflect random noise in the data, here defined as the change in the measured $\langle v \rangle$ introduced by a change in the chosen flux cutoff in the first moment map.

The overall error in the measurement of $\Omega_\mathrm{p}(r)$ given by the best-fit global model solution is defined relative to systematic errors in the calculation. Uncertainty in the assumed position angle (PA), for example, has the largest potential for introducing errors into $\langle v \rangle_i$, or conversely, the b_i in Eq. 1, and is the dominant source of error in TW calculations (Debattista

2003; Meidt et al. 2008a). We assess this error by testing the sensitivity of the solutions to departures from the nominal value for the PA; all reported error bars reflect the influence of PA uncertainty alone (inclination errors, for instance, are here negligible in comparison).

3. Application to M51

3.1. Observations

We apply the TWR method to the disk of M51 traced by high resolution CO observations from the BIMA Survey of Nearby Galaxies (SONG; Helfer et al. 2003). A complete description of the data can be found in Shetty et al. (2007). The 2-σ zeroth and first moment maps used in this analysis, derived from the full BIMA cube, are shown in Fig. 1. Measurement errors given by uncertainty in the flux-cutoff are defined relative to maps at the 1- and 3-σ levels.

According to the arguments of Zimmer et al. (2004) and Rand & Wallin (2004), CO emission, the standard tracer of the molecular component of the ISM, suitably meets the TW assumptions for galaxies where the ISM is everywhere dominated by molecular gas. Since in these data molecular hydrogen is found dominant over the majority of the CO emitting disk (roughly $R < 105''$), with $N(H_2)/N(HI) \sim 10$ (Shetty et al. 2007) assuming a conversion factor between CO intensity and H_2 column density $X = 2 \times 10^{20}\,\mathrm{cm}^{-2}\,[\mathrm{K\,km\,s}^{-1}]^{-1}$, we assert that these observations arguably meet the continuity requirement of the method.

Variation in the X-factor, which Zimmer et al. (2004) found produces a negligible effect on TW estimates for the case of M51, also does not significantly alter the TWR solutions (Meidt et al. 2008b).

3.2. Defining the quadrature and developing testable models

We apply Eq. 1 with regularization using slices spaced at the limiting resolution of the map ($\sim 4''$ at the innermost radii), which at inclination angle i corresponds to a radial bin width $\Delta r = \Delta y/\cos i = 0.23$ kpc ($D = 9.5$ Mpc). Since with the majority of our analysis of M51 we are most interested in characterizing the pattern speeds of the bright spiral structure, this choice is expected to yield high quality solutions for the pattern speeds in this region in particular.

Table 1. Parameters used in the TWR calculation.

Parameter	Value
Kin. Center RA (α) (J2000)	$13^h\,29^m\,52.71^s$
Kin. Center DEC (δ) (J2000)	$47^\circ\,11'\,42.80''$
Distance	9.5 Mpc
Systemic Velocity (V_{sys})	469 km s^{-1} (LSR)
Position Angle	$170^\circ \pm 5^\circ$
Inclination	$24^\circ \pm 3^\circ$

For the kinematic parameters of M51 we combine both our own derivations (using the Groningen Image Processing System (GIPSY) program ROTCUR) and those from Shetty et al. (2007). These parameters are listed in Table 1 and are consistent with most previous determinations.

According to the arguments in Meidt et al. (2008a), we extend the unique quadrature established with the values in Table 1 out to the map boundary $R_{\max} = y_{\max}/\cos i = 7.3$ kpc in order to insure that all information critical for characterizing the patterns of interest is accounted for. To minimize the risk of regularization-induced bias in solutions $\Omega_p(r)$ given this fairly extensive quadrature (described in Meidt et al. 2008a), we identify susceptible regions and calculate bins there without regularization. This imposes the additional parametrization of a cut radius r_c on our model solutions, interior to which regularization proceeds as defined in Meidt et al. (2008a).

Evidence for regions in the outer disk of M51 susceptible to regularization-induced bias is identifiable a priori in the surface brightness (Fig. 1) and its Fourier decomposition (Fig. 2). In the region outside $r \sim 4$ kpc, in particular, where both the surface brightness and power in the $m = 2$ component are low, the information to be extracted there is potentially unreliable and difficult to constrain through modeling.

We therefore consider models which parametrize a cut radius at both $r_c = 4.1$ kpc and at $r_c = 5.3$ kpc. In testing, we find the former to coincide with a clear minimum in the χ^2, with all other best-fit parameters held fixed. The latter, which corresponds to a second, shallower minimum, is a compelling location for the separation between the inner and outer spiral arms, since it seems to match expectations for the location where the outer, material pattern begins (see Tully 1974; Elmegreen et al. 1989; Vogel et al. 1993; Salo & Laurikainen 2000a). In order to test for the possibility of multiple pattern speeds and/or winding, models additionally parametrize either single or multiple distinct radial domains within which the solution can vary as zeroth, first or second order polynomials.

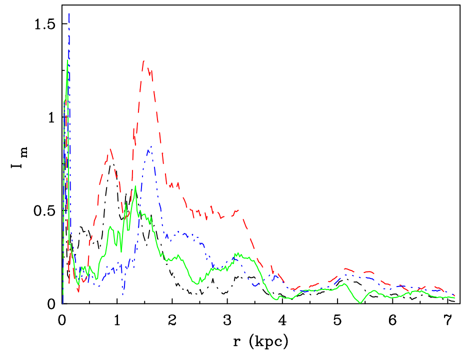

Fig. 2. Fourier power spectrum of the moment zero map shown in Fig. 1. Modes up to $m = 5$ are plotted as a function of radius ($m = 1$ in black dash-dot, $m = 2$ in red dash, $m = 3$ in green solid, $m = 4$ in blue dash-dot-dot-dot, and $m = 5$ in purple dot line).

4. M51: Results

4.1. Best-fit models

Although the procedure outlined in the previous section prevents us from constraining the outermost pattern speed, calculating the outer bins without regularization in principle improves the accuracy with which the solution for the inner disk can realize the true pattern speed. In doing so, we find the data at the nominal PA to be well fit by two distinct pattern speeds interior to $r_c = 4.1$ kpc. The overall pattern speed solution with PA uncertainty $\delta_{PA} = \pm 5°$ is represented in Fig. 3. Error bars represent the dispersion of the parameters in the best-fit solution derived with a two-pattern speed model at PA = 165°, 170°, and 175°. As will be discussed further in Sect. 4.2, these two pattern speeds both end at corotation, within the uncertainties. When the regularized zone $4.1 < r < 5.3$ kpc is included in solutions, the best-fit solution once again measures two pattern speeds inside 4 kpc, but now a third, distinct pattern speed is also parametrized. In this solution, the two pattern speeds measured inside $r \simeq 4$ kpc are nearly identical to the values measured in solutions with $r_c = 4.1$ kpc. This seems to suggest that the determination in the third zone is fairly accurate, despite the evidence in Figs. 1 and 2 that information beyond $r \simeq 4$ kpc is not conducive to modeling and extraction. Also, the pattern speed in the zone $4 \lesssim r \lesssim 5$ kpc, $\Omega_{p,3} = 20$ km s^{-1} kpc^{-1}, is in fact lower than all measurements interior. Presumably, the value in this zone contributes to the measurement of the rather low TW value 38 km s^{-1} kpc^{-1} (Zimmer et al. 2004).

As reported in Meidt et al. (2008b), all χ^2 are lower in solutions with $r_c = 4.1$ kpc than with $r_c = 5.3$ kpc, and so, the analysis at best indicates that within $r_c = 4.1$ kpc the data at the nominal PA are well fit by two pattern speeds. In addition, though, it seems possible to extend the multi-speed model's estimate for $\Omega_p(r)$ to 5.3 kpc without loss of validity, and this appears to be a good approximation to the pattern speeds of the structure across this zone.

4.1.1. PA dependence

This same analysis applied to each PA separately (without restricting the form of solutions at PA = 165° and 175° to those optimal at PA = 170°, which was used to define the errors in the previous section) indicates that the values and domains of the best-fit pattern speeds vary from PA to PA. Most notably, at 175° only a single, constant pattern speed is measured inside $r \sim 4$ kpc (Meidt et al. 2008b).

As discussed in Meidt et al. (2008b), given the rather large PA uncertainty this measure-

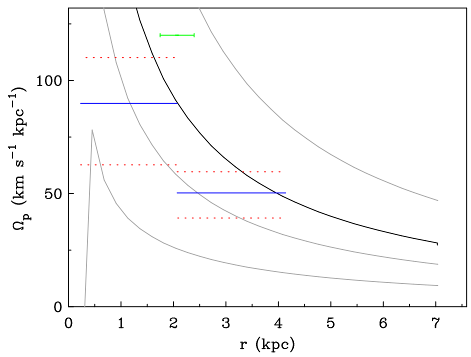

Fig. 3. The best-fit regularized solution with r_c = 4.1 kpc for PA = 170° ± 5°. For this solution, bins exterior to r = 4.1 kpc (not shown) have been calculated without regularization. Dashed red lines represent the difference from solutions derived with a two-pattern speed model at PA = 165° and 175°. The horizontal error bar represents the dispersion in $r_{t,1}$, the location of the transition between the two pattern speeds, from PA to PA. The values in the zone of the bright spiral structure correspond to $\Omega_{p,1} = 90^{+20}_{-27}$ km s^{-1} kpc^{-1} out to $r_{t,1}$ = 2.1 ± 0.3 kpc and $\Omega_{p,2} = 50^{+9}_{-11}$ km s^{-1} kpc^{-1} out to r_c. Fitted curves for Ω, $\Omega \pm \kappa/2$ and $\Omega - \kappa/4$ are shown in gray.

ment is arguably consistent with resulting from a difference in the projection of asymmetries (both intensity and velocity) from that in the 170° case. Critically, however, the data admit both PA = 170° and PA=175°, and according to the findings of Shetty et al. (2007), the latter may be more valid at the inner radii than PA = 170° derived with ROTCUR.

4.2. Possible complimentary evidence for multiple pattern speeds and indications of mode coupling

Although the accuracy of the description provided by two pattern speeds may depend on whether PA = 170° or PA = 175° is more accurate, we find remarkable agreement between the characteristics of the two speeds inside 4 kpc at PA = 170° (Fig. 3) and other evidence in the inner disk in the zone of the bright spiral structure consistent with multiple pattern speeds.

As reviewed by Meidt et al. (2008b), at least two sections best fit with different pitch angles i_p have been identified in both spiral arms, possibly the signature of two or more distinct pattern speeds. Patrikeev et al. (2006) find a maximum in i_p occurring nearly symmetrically in both arms at $r \sim 2$ kpc (see Figs. 6, 7a, and 8a in Patrikeev et al. 2006), very near the transition r_t identified in our best-fit solution at PA = 170°. The transition between the two patterns inside $r \simeq 4$ kpc also coincides with features in the zeroth moment map's Fourier decomposition (Fig. 2); as at $r \sim 4$ kpc, the power in the $m = 2$ mode is characterized by a decline at $r \sim 2$ kpc possibly marking the termination of a distinct structure. (The same can be inferred at the transition between the second and third pattern speeds in the solution with r_c = 5.3 kpc.) In addition, both pattern speeds inside r_c = 4.1 kpc end at corotation within the uncertainties, as demonstrated in Meidt et al. (2008b) with fitted curves for Ω, $\Omega - \kappa/2$, $\Omega - \kappa/4$, and $\Omega + \kappa/2$ plotted here in Fig. 3. This circumstance is consistent with an early prediction for where spirals terminate (i.e., Lin 1970), which later yielded to findings that spirals can extend as far as OLR, if sometimes faintly (see Zhang & Buta 2007 and references therein).

The measured pattern speeds also seem to overlap at resonances and may be consistent with origins in non-linear mode coupling (e.g., Tagger et al. 1987). The most promising instance is that demonstrated by the overlap between CR of $\Omega_{p,1}$ and the UHR of the pattern with $\Omega_{p,2}$ (in Fig. 3). Such coincidences have been identified in simulations where, as in the simulated barred spirals of Rautiainen & Salo (1999), they allow for the transfer of energy and angular momentum from bar to spiral (but see the discussion in Meidt et al. 2008b). Fig. 3 also exhibits a turnover in the curve $\Omega - \kappa/2$, indicating that patterns with angular speeds above the maximum lack an ILR. This suggests that a (trailing) wave with $\Omega_{p,1}$ can reflect from the center as a leading structure, a circumstance complimentary to the Scoville et al. (2001) HST observations of central leading waves, as pointed out by Salo & Laurikainen (2000a).

5. Conclusion

In this paper we present regularized TWR solutions for the pattern speed of the bright spiral structure in the inner disk of M51 derived using high-resolution CO observations that trace the ISM-dominant molecular component. Our primary result is the measurement inside 4 kpc of two pattern speeds, both significantly higher, and together fitting the data better, than the constant global measure of Zimmer et al. (2004) at the nominal PA = 170°. These two pattern speeds both end at corotation within the uncertainties. Since it is in no way imposed by the method, this dynamically reasonable scenario tends to give us confidence as to the physical plausibility of the pattern speeds returned by the analysis.

Future high-resolution and sensitivity CARMA observations of M51 should afford TWR calculations with finer radial bins, thereby allowing for the parametrization of more distinct radial zones, if present. This will either confirm our solutions for $\Omega_{\rm p}(r)$ or demonstrate that solutions describe a succession of many discrete patterns, similar to the transient structures in the Salo & Laurikainen (2000a) model, or simply a winding, material pattern (not indicated here).

Despite the lingering ambiguity in the PA, these TWR solutions present a new picture of the bright spiral structure of M51, one that should prompt tests of long-lived density wave theories in other nearby grand-design spirals. Continued tests of the relation between multiple spiral pattern speeds in a single disk and spiral winding/longevity will be the subject of upcoming work.

Acknowledgements. SEM acknowledges support from a NASA-funded New Mexico Space Grant Consortium Graduate Research Fellowship. This material is based upon work supported by the National Science Foundation under grant AST 08-07032 to RJR. MRM gratefully acknowledges the support of an STFC Senior Fellowship.

References

Debattista, V. P. 2003, MNRAS, 342, 1194
Elmegreen, B. G., Elmegreen, D. M., & Seiden, P. E. 1989, 343, 602
Garcìa-Burillo, S., Combes, F., & Gerin, M. 1993, A&A, 274, 148
Helfer, T. T., Thornley, M. D., Regan, M. W., et al. 2003, ApJS, 145, 259
Howard, S., & Byrd, G. G. 1990, AJ, 99, 1798
Lin, C. C. 1970, in The spiral structure of our galaxy, IAU Symp. 38, ed. W. Becker, & G. I. Contopoulos (Reidel, Dordrecht), 377
Lin, C. C., & Shu, F. H. 1964, ApJ, 140, 646
Meidt, S. E., Rand, R. J., Merrifield, M. R., Debattista, V. P., & Shen, J. 2008a, ApJ, 676, 899
Meidt, S. E., Rand, R. J., Merrifield, M. R., Shetty, R., & Vogel, S. 2008b, ApJ, 688, 224
Merrifield, M. R., Rand, R. J., & Meidt, S. E. 2006, MNRAS, 366, 17
Patrikeev, I., Fletcher, A., Stepanov, R. et al. 2006, A&A, 458, 441
Rand, R. J. 1993, ApJ, 410, 68
Rand, R. J., & Wallin, J. F. 2004, ApJ, 614, 142
Rautiainen, P., & Salo, H. 1999, A&A, 348, 737
Salo, H., & Laurikainen, E. 2000, MNRAS, 319, 377
Scoville, N. Z., Polletta, M., Ewald, S., et al. 2001, AJ, 122, 3017
Shetty, R., Vogel, S. N., Ostriker, E. C., & Teuben, P. J. 2007, ApJ, 665,1138
Tagger, M., Sygnet, J. F., Athanassoula, E., & Pellat, R. 1987, ApJ, 318, L43
Toomre, A., & Toomre J. 1972, ApJ, 178, 623
Tully, R. B. 1974, ApJS, 27, 449
Tremaine, S., & Weinberg, M. D. 1984, ApJ, 282, L5
Vogel, S. N., Rand, R. J., Gruendel, R. A., & Teuben, P. J. 1993, PASP, 105, 60
Zhang, Z., & Buta, R. J. 2007, AJ, 133, 2584
Zimmer, P., Rand, R. J., & McGraw, J. T. 2004, ApJ, 607, 285